Acoustic response of a laser-excited polycrystalline Au-film studied by ultrafast Debye–Scherrer diffraction at a table-top short-pulse x-ray source

Cite as: AIP Advances 10, 035015 (2020); doi: 10.1063/1.5142220
Submitted: 11 December 2019 • Accepted: 26 February 2020 •
Published Online: 12 March 2020

W. Lu,[a] M. Nicoul, U. Shymanovich, F. Brinks, M. Afshari, A. Tarasevitch, D. von der Linde, and K. Sokolowski-Tinten[b]

AFFILIATIONS

Faculty of Physics and Centre for Nanointegration Duisburg-Essen, University of Duisburg-Essen, Lotharstrasse 1, 47048 Duisburg, Germany

[a]**Now at**: European X-Ray Free-Electron Laser Facility, Holzkoppel 4, 22869 Schenefeld, Germany.
[b]**Author to whom correspondence should be addressed:** klaus.sokolowski-tinten@uni-due.de

ABSTRACT

The transient acoustic response of a free-standing, polycrystalline thin Au-film upon femtosecond optical excitation has been studied by time-resolved Debye–Scherrer x-ray diffraction using ultrashort Cu K_α x-ray pulses from a laser-driven plasma x-ray source. The temporal strain evolution has been determined from the transient shifts of multiple Bragg diffraction peaks. The experimental data are in good agreement with the results of calculations based on the two-temperature model and an acoustic model assuming uniaxial strain propagation in the laser-excited thin film.

I. INTRODUCTION

Due to the rapid progress in the development of short-pulse x-ray and electron sources, the field of ultrafast structural dynamics has seen dramatic progress in the last two decades (e.g., Refs. 1 and 2 and references therein). With respect to x rays, large-scale facilities such as x-ray free electron lasers (XFELs) define the current state-of-the-art,[3–5] but laser-plasma based x-ray sources still represent an interesting alternative due to their simplicity, versatility, low cost, and accessibility. In fact, these table-top, lab-scale sources have enabled the first ultrafast (i.e., femtosecond) time-resolved x-ray diffraction experiments (e.g., Refs. 6–9) and are still the subject of intense development to improve their efficiency[10] or to reach higher photon energies.[11–13]

Due to their comparably much lower x-ray flux, these sources have been mainly used to study single-crystalline materials that provide strong diffraction signals in a reflective Bragg-geometry. However, laser-pump x-ray probe experiments often require thin film samples to match the thickness of the optically excited layer to the x-ray probing depth. Since not all materials can be grown as high quality single crystals in thin film form, the range of materials that can be studied with this approach is limited.

In contrast, for most materials, polycrystalline films can be prepared more easily. In this case, the random orientation of crystallites in the sample allows us to use the well-known Debye–Scherrer scheme.[14] While the scattering signal is distributed over a diffraction ring (instead of localized diffraction spots), this scheme represents a much simpler approach since no precise sample adjustments (i.e., Bragg-angle) are necessary, and the signal of several Bragg-peaks can be recorded simultaneously. Enabled by the large scattering cross section of electrons in the keV to MeV energy range, Debye–Scherrer diffraction is routinely applied in ultrafast electron diffraction experiments (e.g., Refs. 15–18). This is also easy to realize at x-ray sources that provide high flux as well as a collimated beam like synchrotron or XFELs, enabling even

single-pulse detection of diffraction patterns with a high signal-to-noise ratio (e.g., Refs. 19–21).

The situation is much more challenging for laser-plasma based x-ray sources not only due to their lower x-ray flux but also because of their spatially incoherent, full-solid-angle emission. Therefore, the use of an appropriate x-ray optic, which collects and (quasi-) collimates the radiation, is mandatory to enable this approach.[22–27] Successful application of ultrafast Debye–Scherrer diffraction at a laser-plasma based x-ray source has recently been demonstrated by measuring transient changes of electron density for thick (10–100 μm) powder samples of ionic crystals.[25,28,29]

Here, we present the application of time-resolved Debye–Scherrer diffraction at a femtosecond laser-plasma based x-ray source for the study of structural dynamics in a thin sample, namely, the acoustic response of a 200 nm, polycrystalline Au-film upon ultrafast optical excitation. Such *coherent acoustic phonons* in thin films have been the subject of many studies using both time-resolved x rays (e.g., Refs. 30–33) and electron diffraction (e.g., Refs. 15, and 34–36) and represent, therefore, an excellent test-case. We determine the transient strain evolution in the sample from the measured changes of the Debye–Scherrer diffraction patterns, in particular, the time-dependent shift of multiple Bragg-peaks. The measured data are in good agreement with calculations using the two-temperature model (TTM) to estimate the time-dependent pressure/stress and an acoustic model assuming uniaxial strain wave propagation in the film.

II. EXPERIMENTAL SCHEME AND DATA

The experiments were performed using a table-top laser-plasma based Cu K_α x-ray source, and the principle scheme of the experimental setup is shown in Fig. 1(a). Short bursts of Cu K_α radiation at 8 keV were produced by focusing femtosecond laser pulses (repetition rate 10 Hz, pulse energy 150 mJ, pulse duration 120 fs, and wavelength 800 nm) onto the surface of a moving 10 μm thick copper tape housed in a small vacuum chamber. A pre-pulse scheme is employed to optimize x-ray production,[37,38] resulting in a total Cu K_α-flux of more than 10^{10} photons per pulse.[39–42]

Since the x rays are emitted into the full solid angle, we used a graded multi-layer Montel-type x-ray mirror[43] to collect the emitted K_α radiation from the backside of the tape target and to image the source onto the sample under study. With a magnification of 5×, more than 10^5 K_α photons per pulse are delivered to the sample in a quasi-collimated beam of 0.23° convergence/divergence and a spot size of about 140 μm. The temporal resolution is better than 300 fs, as evidenced by experiments investigating faster material responses (i.e., coherent acoustic phonons on Bi[44,45]).

The sample—a 200 nm free-standing polycrystalline Au-film supported by a Ni-mesh[46]—is optically excited by a small fraction split off from the main laser beam. With a laser spot diameter (FWHM) of 400 μm on the sample, which is approximately 3× larger than that of the x-ray probe beam, the measured x-ray signals represent the response of a homogeneously excited region. Transient diffraction patterns, typically accumulated over 3000 pulses (5 min integration time), were recorded with a single-photon sensitive phosphor-based x-ray area detector (Photonic Science X-Ray Gemstar HS) as a function of time delay between the optical pump pulse (peak fluence ≈ 160 mJ/cm^2) and the x-ray probe. In order to simultaneously record as many diffraction orders as possible, the detector was placed close to the sample (distance 38 mm) and not normal to the direct x-ray beam, but at a shallow angle of 28°. This allowed us to cover an angular range of $35° \le \theta \le 82°$

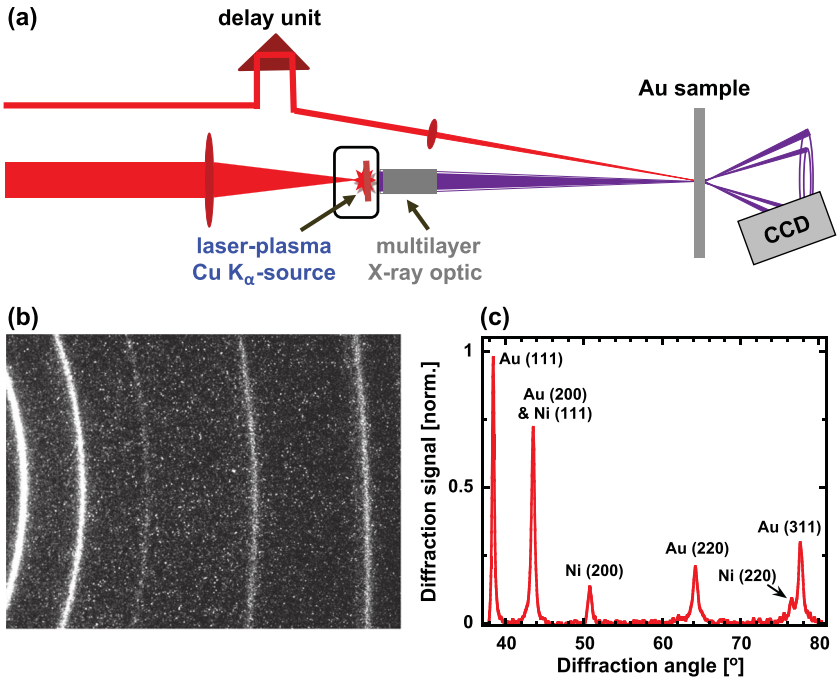

FIG. 1. (a) Scheme of the experimental setup. (b) Typical diffraction pattern of the 200 nm polycrystalline Au-film recorded with an x-ray area detector. (c) Diffraction profile $I(\theta)$ obtained by azimuthal integration of the diffraction pattern in (b).

[θ: diffraction angle measured with respect to the incoming x-ray beam; see also Fig. 3(a)].

A typical Debye–Scherrer diffraction pattern of the Au-film, as recorded with the x-ray area detector, is depicted in Fig. 1(b). The corresponding diffraction profile $I(\theta)$, obtained by azimuthal integration, is presented in Fig. 1(c). The four lowest order diffraction peaks of Au can be clearly identified, as well as some (weaker) diffraction peaks of the supporting Ni-mesh [all diffraction peaks are labeled with their Miller indices in Fig. 1(c)]. The two higher order peaks exhibit a width (FWHM) of about 0.7°. We attribute this to the finite grain size in the Au-film. By using Scherrer's equation[47] (with form-factor K = 1) and taking into account the x-ray spot size and the finite spectral width of the K_α emission, we obtain a crystallite size of about 15–20 nm,[48] in line with the observation of smooth, continuous diffraction rings.

In the analysis of the time-resolved data, we focused on the two higher order diffraction peaks, namely, the (220)- and the (311)-reflection, because of the larger magnitude of the laser-induced changes as compared to the low order peaks. For the (111)-reflection, we determined only the maximum shift [see Fig. 3(b)], while the (200)-reflection could not be properly analyzed due to overlap with the Ni (111)-reflection. The results are presented in Fig. 2(a), which shows a zoom-in view of the diffraction profiles $I(\theta)$ of the (220)- and (311)-reflection without (blue data points) and with (red data points) laser-pumping at a pump-probe time delay of 70 ps.

Upon pumping, both diffraction peaks shift toward smaller diffraction angles. To quantify the shift, the Bragg-peaks have been fitted by a Gaussian function. However, to eliminate any effects on the fitting due to the noisy background as well as the adjacent Ni (220)-peak, only data points with an intensity of above 30% of the corresponding peak maximum have been used for fitting. While this procedure allows determination of the peak position, the area under the peak, representing the integrated diffraction efficiency of the particular reflection, cannot be accurately determined.[49–51] The results of such fits are shown as red (with pump) and blue (without pump) solid lines in Fig. 2(a). The derivative-like shape of the difference in these fits [green solid curve in Fig. 2(a)] emphasizes that the peak shift represents the main pump-induced effect, and the following analysis will focus on this.

Figure 2(b) shows the angular shift (red data points) of the (220) (top) and (311) Bragg-peaks as a function of time delay, as obtained from the fitting procedure described above (errors bars represent the fitting errors). The blue data points are the results of reference measurements without pumping made over the course of the experiment at the given delay setting. The dashed curves are guides to the eye. The temporal evolution of the angular position of both diffraction peaks exhibits a pronounced oscillatory behavior with a half-period of (67 ± 1) ps. As will be discussed in Sec. III, this can be attributed to strain waves propagating back and forth in the thin Au-film.

III. STRAIN ANALYSIS AND MODELING

A shift of the diffraction peaks toward smaller diffraction angles indicates lattice expansion, i.e., positive strain $\eta = \Delta d_{hkl}/d_{hkl}$ (d_{hkl}: lattice constant). This expansion is driven by a fast, laser-induced increase of pressure, which has electronic and thermal contributions,[52] as will be outlined in more detail below. Relaxation of the excess pressure/stress occurs by one-dimensional, longitudinal strain waves propagating normal to the surface[53] because the nominal film thickness of 200 nm is much smaller than the laser-excited area (diameter 400 μm). To deduce the transient strain from the measured peak shift, one needs to consider that in the Debye–Scherrer configuration, scattering at a particular scattering angle θ occurs by a subset of all crystallites which are oriented such that the Bragg-condition is fulfilled for a particular Bragg-peak (hkl) with $\Theta = 2\Theta_B$. The corresponding scattering diagram is depicted in Fig. 3(a).

Herein, $\vec{k}_{in}$ and $\vec{k}_{out}$ (gray) denote the wave-vector of the incoming and scattered x rays, respectively. Their end-points lie on the so-called Ewald-sphere (gray circle). For a polycrystalline sample with randomly oriented crystallites, the corresponding reciprocal lattice vectors $\vec{G}_{hkl}$ lie on a sphere with radius G_{hkl} (red circle). Where this sphere cuts the Ewald-sphere, the Bragg-condition is fulfilled, leading to scattering at $\Theta = 2\Theta_B$.

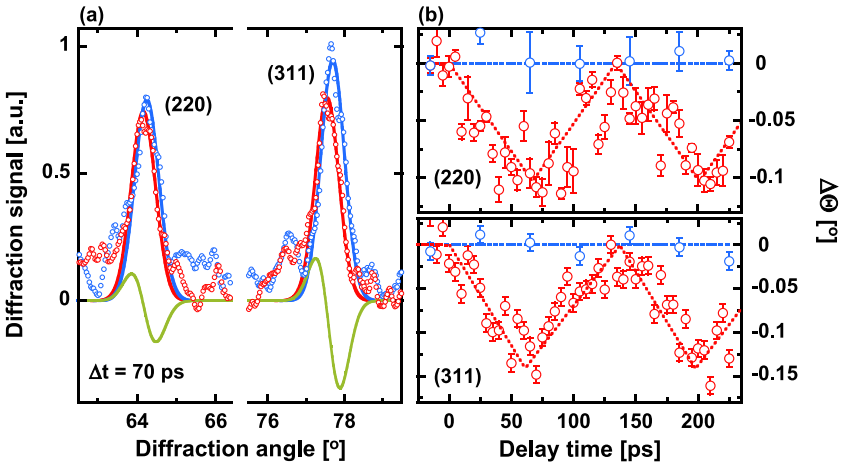

FIG. 2. (a) Diffraction profiles $I(\theta)$ of the (220)-reflection (left) and (311)-reflection (right) without (blue) and with (red) laser-pumping (pump-probe time delay Δt = 70 ps). Open circles: experimental data; solid lines: Gaussian fits; green solid curve: difference in the fitting results with (red curve) and without (blue curve) pumping. (b) Angular shift of the (220)-reflection (top) and (311)-reflection (bottom) as a function of pump-probe time delay obtained from the Gaussian fitting of the diffraction peaks. Red data points: with pumping; blue data points: reference data without pumping measured over the course of the experiment at the given delay setting. The dashed curves are guides to the eye.

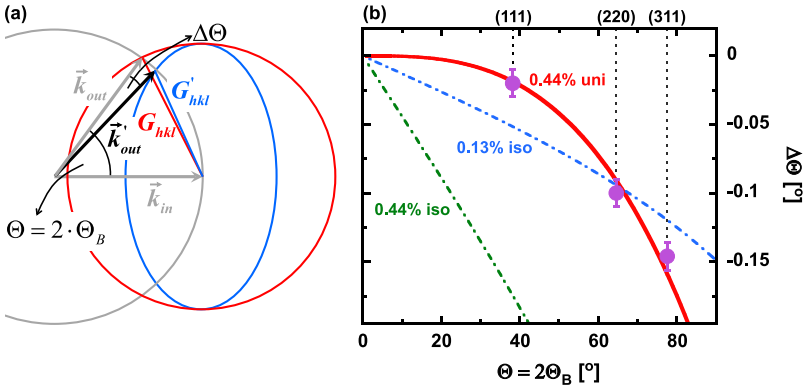

FIG. 3. (a) Ewald-sphere (gray circle) construction for diffraction from a polycrystalline sample without strain (red circle) and with uniaxial strain along the surface normal (blue ellipse). (b) Angular shift of the diffraction peaks as a function of diffraction angle. Violet dots: experimental data for the (111)-, (220)-, and (311)-reflections; green and blue-dashed curves: calculated shift assuming isotropic strain of 0.44% (green) and 0.13% (blue), respectively; red solid curve: shift calculated according to Eq. (1) assuming a uniaxial strain of 0.44% along the surface normal.

When the film is uniaxially expanded ($\eta > 0$) along the surface normal, which equals the direction of $\vec{k}_{in}$, the sphere with radius G_{hkl} is compressed in this direction into an ellipsoid (blue) with a short axis $(1 - \eta) \cdot G_{hkl}$. Now, the Bragg-condition is fulfilled, where this ellipsoid cuts the Ewald-sphere corresponding to a differently oriented subset of crystallites. Scattering, therefore, occurs in a different direction $\vec{k}'_{out}$ (black), leading to an angular shift $\Delta\theta$. According to Fig. 3(b), simple geometrical considerations lead to:[19,45]

$$\Delta\Theta = -\eta \cdot \frac{(1 - \cos\Theta)^2}{\sin\Theta}. \quad (1)$$

Figure 3(b) compares the measured maximum shift of the (111)-, (220)-, and (311)-reflection [violet data points; the (200)-peak could not be analyzed due to overlap with the strong (111)-peak of Ni] to calculations for different strain conditions. The blue and green-dashed curves represent the expected angular shifts assuming isotropic strains of 0.13% (blue) and 0.44% (green) ($\Delta\Theta = -\tan\Theta \cdot \eta$), respectively, which are obviously unable to describe the measured data. In contrast, good agreement is found using Eq. (1) with a strain of 0.44% (red solid curve), giving clear evidence that the laser-driven expansion of the film is indeed uniaxial. Applying Eq. (1) to the measured time-dependent shifts of the (220)- and (311)-peaks [compare Fig. 2(b)], the strain as a function of pump-probe time delay can be obtained, as depicted in Fig. 4(a). Similar to the measured angular shifts, the time-dependent strain exhibits an undamped (over the measured delay range) oscillatory behavior with a half-period of (67 ± 1) ps.

As mentioned above, this oscillatory behavior is caused by strain waves traveling back and forth in the Au-film. The half-period of t_{ac} = (67 ± 1) ps corresponds to the time such a strain wave needs to propagate (with the speed of sound c_S) through the full film thickness d once. With c_S = 3.24 km/s for polycrystalline Au,[54] this allows us to determine the actual film thickness $d = c_S \cdot t_{ac}$ = (217 ± 3) nm, in good agreement with the nominal film thickness and the ±10% thickness tolerance specified by the manufacturer.

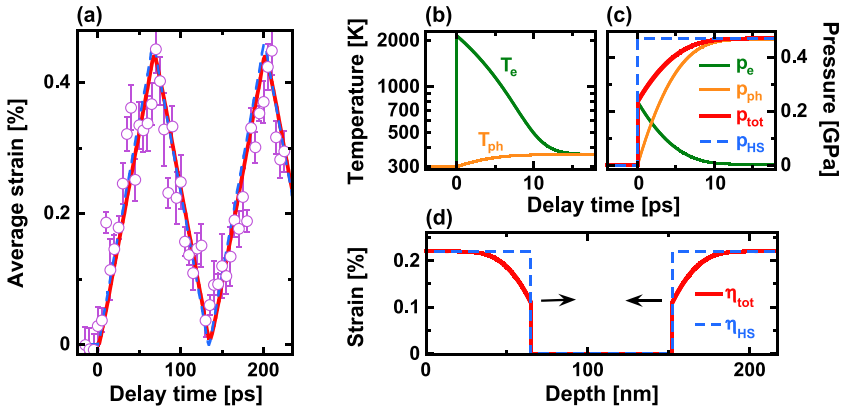

FIG. 4. (a) Average strain as a function of pump-probe time delay (red open circles: experimental data; red solid curve: calculation results [see (b)–(d)] with fully time-dependent pressure; blue-dashed curve: calculation results assuming an instantaneous increase of pressure). (b) Electron (green) and lattice (orange) temperature as a function of time calculated using the TTM. (c) Resulting time-dependent pressure contributions (green: electronic pressure p_e, orange: thermal pressure p_{ph}, red: total pressure $p_{tot} = p_e + p_{ph}$). The blue-dashed curve represents a simplified instantaneous pressure increase. (d) Spatial dependence of the strain in the film 20 ps after excitation. The red solid curve is the result with the fully time-dependent pressure, as shown in (c); the blue-dashed curve corresponds to the instantaneous increase of pressure. The arrows mark the propagation direction of the strain pulses.

To quantitatively model the response of the Au-film, we applied the two-temperature model[55] (TTM) in combination with solution of one-dimensional elastic equations.[53] The relevant TTM-parameters are a constant lattice specific heat of C_{ph} = 2.5 MJ/(m^{3}K),[54] an electronic specific heat $C_e(T_e) = A_e \cdot T_e$ with A_e = 67.6 J/(m^3 K^2),[52] and an electron-phonon coupling parameter $g = 1.7 \times 10^{16}$ W/(m^{3}K).[56] For simplicity, we assume that laser excitation leads to an (i) instantaneous and (ii) spatially homogeneous increase of the electronic temperature in the film, which is justified by (i) the relatively weak electron-phonon coupling, leading to correspondingly *long* electron-lattice equilibration times of a few ps,[16,56] and (ii) the very efficient, ballistic/superdiffusive electronic transport in Au.[57,58] Results of such calculations are shown in Fig. 4(b) for an asymptotic rise in lattice temperature $\Delta T_{ph,\infty}$ = 61 K (see below), corresponding to an initial electron temperature $T_{e,max}$ = 2153 K.

The changes in both the electronic and lattice temperatures cause an increase in pressure (isotropic stress) in the material, which can be expressed as[52] $\delta P = \gamma_e C_e \delta T_e + \gamma_{ph} C_{ph} \delta T_{ph}$. Herein, γ_e and γ_{ph} denote the electronic and lattice Grüneisen parameters, respectively, with $\gamma_{ph} = 3$[59] and $\gamma_e/\gamma_{ph} \approx 0.5$.[32] The resulting time-dependent electronic (p_e) and thermal (p_{ph}) pressure contributions are depicted in Fig. 4(c) as the green and orange curve, respectively. The total pressure $p_{tot} = p_e + p_{ph}$ (red curve) is then used to solve the one-dimensional elastic equations.[53] In this model, the peak strain is given by

$$\eta_{max} = \frac{6B\beta}{c_S^2 \rho} \cdot \Delta T_{ph,\infty}. \quad (2)$$

Herein, B = 177 GPa denotes the bulk modulus,[60] $\beta = 1.426 \times 10^{-5}$ K^{-1} is the linear thermal expansion coefficient,[60] ρ = 19.3 g/cm^3 is the density, and c_S = 3.24 km/s is the sound velocity[54] of Au. Equation (2) together with the measured η_{max} = 0.44% results in $\Delta T_{ph,\infty}$ = 61 K, the value that has been used in the TTM-calculations.

Results of the acoustic modeling are presented in Fig. 4(d), which shows the calculated strain profile at Δt = 20 ps. Since the experiments have been carried out on a free-standing film, strain waves with an equal amplitude of $0.5 \cdot \eta_{max}$ are launched at both film surfaces, which propagate into the film. At the chosen time of Δt = 20 ps, they have traveled less than 1/3 of the film thickness and are, therefore, still spatially separated. The spatial shape of each pulse reflects the temporal evolution of the total pressure p_{tot}. At later times, both pulses overlap and when approaching the opposite (free) surface, they are reflected with a sign change (wave reflection at an open end).

Since the time-dependent spatial strain distribution is inhomogeneous, the changes in the x-ray diffraction patterns are characterized by angular shifts as well as changes in shape (e.g., broadening) of the rocking curves of individual diffraction peaks.[32] However, due to the large angular width of the Bragg-peaks of about 0.7° in our experiment, such shape changes of the rocking curves cannot be resolved. As a result, the measured shifts represent the average strain in the film at a given time, as presented in Fig. 4(a). The average strain, as determined from the acoustic model calculations [red solid curve in Fig. 4(a)] agrees very well with the experimental data.

Over the measured delay range and within the accuracy of the measurements, the strain oscillations are undamped, as has been already emphasized above. While some damping might be expected due to the polycrystalline film structure and has been observed in ultrafast electron diffraction studies on much thinner (20 nm) metal films,[15,34] the apparently undamped character is a consequence of having a free-standing film as the sample, where the acoustic pulses exhibit total reflection at the free surfaces. In contrast, strain waves in thin films on substrates are partially (depending on the difference in acoustic impedance between the film and substrate) transmitted into the substrate upon each round-trip and usually experience, therefore, much stronger damping.[32]

We also performed the acoustic modeling with a simplified pressure evolution, namely, an instantaneous increase at Δt = 0 (equivalent to infinitely fast electron-phonon coupling and/or equal Grüneisen parameters), as indicated by the blue-dashed curve in Fig. 4(c). The resulting strain pulses (now exhibiting a rectangular shape) and the corresponding time-dependence of the average strain are depicted by the blue-dashed curves in Figs. 4(d) and 4(a), respectively. With the given accuracy, our current data do not allow to discriminate between the two scenarios. However, our previous experiments on an epitaxial Au-film[32] provided clear evidence that the finite electron-phonon coupling and the difference of the Grüneisen parameters need to be taken into account to properly interpret the observed acoustic response.

IV. SUMMARY

In summary, we have used ultrafast time-resolved Debye–Scherrer diffraction to study the acoustic response of a free-standing polycrystalline Au-film upon femtosecond optical excitation. From the measured shifts of different Bragg-peaks, the transient strain evolution in the film has been determined, which follows the behavior expected from longitudinal acoustic waves propagating normal to the surface of the free-standing sample. Very good quantitative agreement is found with the results of calculations based on the two-temperature model and solution of the one-dimensional acoustic equations taking into account electronic and thermal contributions to the laser-induced pressure/stress. Our results demonstrate the feasibility of time-resolved Debye–Scherrer diffraction experiments on thin solid samples (where film thickness and excitation depth are matched) using a laser-plasma based x-ray source. This considerably extends the range of materials for which Debye–Scherrer diffraction at such sources can be applied, in particular, when future prospects to increase their efficiency[10] are considered.

ACKNOWLEDGMENTS

Financial support by the *Deutsche Forschungsgemeinschaft* (DFG, German Research Foundation) through project C01 *Structural Dynamics in Impulsively Excited Nanostructures* of the Collaborative Research Center (Project No. SFB 1242) and *Non-Equilibrium Dynamics of Condensed Matter in the Time Domain* (Project No. 278162697) is gratefully acknowledged. We also acknowledge support by the Open Access Publication Fund of the University of Duisburg-Essen.

REFERENCES

[1] R. Schoenlein, T. Elsaesser, K. Holldack, Z. Huang, H. Kapteyn, M. Murnane, and M. Woerner, "Recent advances in ultrafast x-ray sources," Philos. Trans. R. Soc., A **377**, 20180384 (2019).

[2]G. Sciaini, "Recent advances in ultrafast structural techniques," Appl. Sci. **9**, 1427 (2019).
[3]C. Bostedt, S. Boutet, D. M. Fritz, Z. Huang, H. J. Lee, H. T. Lemke, A. Robert, W. F. Schlotter, J. J. Turner, and G. J. Williams, "Linac coherent light source: The first five years," Rev. Mod. Phys. **88**, 015007 (2016).
[4]M. Dunne, "X-ray free-electron lasers light up materials science," Nat. Rev. Mater. **3**, 290 (2018).
[5]H. N. Chapman, "X-ray free-electron lasers for the structure and dynamics of macromolecules," Annu. Rev. Biochem. **88**, 35 (2019).
[6]C. Rischel, A. Rousse, I. Uschmann, P.-A. Albouy, J.-P. Geindre, P. Audebert, J.-C. Gauthier, E. Förster, J.-L. Martin, and A. Antonetti, "Femtosecond time-resolved x-ray diffraction from laser-heated organic films," Nature **390**, 490 (1997).
[7]C. Rose-Petruck, R. Jimenez, T. Guo, A. Cavalleri, C. W. Siders, F. Raksi, J. A. Squier, B. C. Walker, K. R. Wilson, and C. P. J. Barty, "Picosecond–milliångström lattice dynamics measured by ultrafast x-ray diffraction," Nature **398**, 310 (1999).
[8]A. Rousse, C. Rischel, S. Fourmaux, I. Uschmann, S. Sebban, G. Grillon, P. Balcou, E. Förster, J. P. Geindre, P. Audebert, J. C. Gauthier, and D. Hulin, "Non-thermal melting in semiconductors measured at femtosecond resolution," Nature **410**, 65 (2001).
[9]K. Sokolowski-Tinten, C. Blome, J. Blums, A. Cavalleri, C. Dietrich, A. Tarasevitch, I. Uschmann, E. Förster, M. Kammler, M. Horn-von Hoegen, and D. von der Linde, "Femtosecond x-ray measurement of coherent lattice vibrations near the Lindemann stability limit," Nature **422**, 287 (2003).
[10]J. Weisshaupt, V. Juvé, M. Holtz, S. Ku, M. Woerner, T. Elsaesser, S. Ališauskas, A. Pugžlys, and A. Baltuška, "High-brightness table-top hard x-ray source driven by sub-100-femtosecond mid-infrared pulses," Nat. Photonics **8**, 927 (2014).
[11]S. Fourmaux and J. C. Kieffer, "Laser-based K_α x-ray emission characterization using a high contrast ratio and high-power laser system," Appl. Phys. B **122**, 162 (2016).
[12]Y. Azamoum, R. Clady, A. Ferré, M. Gambari, O. Utéza, and M. Sentis, "High photon flux K_α Mo x-ray source driven by a multi-terawatt femtosecond laser at 100 Hz," Opt. Lett. **43**, 3574 (2018).
[13]Y. Azamoum, V. Tcheremiskine, R. Clady, A. Ferré, L. Charmasson, O. Utéza, and M. Sentis, "Impact of the pulse contrast ratio on molybdenum K_α generation by ultrahigh intensity femtosecond laser solid interaction," Sci. Rep. **8**, 4119 (2018).
[14]P. Debye and P. Scherrer, "Interferenz an regellos orientierten Teilchen im Röntgenlicht. I," Phys. Z. **17**, 277 (1916).
[15]S. Nie, X. Wang, H. Park, R. Clinite, and J. Cao, "Measurement of the electronic Grüneisen constant using femtosecond electron diffraction," Phys. Rev. Lett. **96**, 025901 (2006).
[16]M. Ligges, I. Rajkovic, P. Zhou, O. Posth, C. Hassel, G. Dumpich, and D. von der Linde, "Observation of ultrafast lattice heating using time resolved electron diffraction," Appl. Phys. Lett. **94**, 101910 (2009).
[17]L. Waldecker, T. Vasileiadis, R. Bertoni, R. Ernstorfer, T. Zier, F. H. Valencia, M. E. Garcia, and E. S. Zijlstra, "Coherent and incoherent structural dynamics in laser-excited antimony," Phys. Rev. B **95**, 054302 (2017).
[18]J. Hu, T. E. Karam, G. A. Blake, and A. H. Zewail, "Ultrafast lattice dynamics of single crystal and polycrystalline gold nanofilms," Chem. Phys. Lett. **683**, 258–261 (2017).
[19]J. S. Wittenberg, T. A. Miller, E. Szilagyi, K. Lutker, F. Quirin, W. Lu, H. Lemke, D. Zhu, M. Chollet, J. Robinson, H. Wen, K. Sokolowski-Tinten, A. P. Alivisatos, and A. M. Lindenberg, "Real-time visualization of nanocrystal solid–solid transformation pathways," Nano Lett. **14**, 1995 (2014).
[20]A. E. Gleason, C. A. Bolme, H. J. Lee, B. Nagler, E. Galtier, D. Milathianaki, J. Hawreliak, R. G. Kraus, J. H. Eggert, D. E. Fratanduono, G. W. Collins, R. Sandberg, W. Yang, and W. L. Mao, "Ultrafast visualization of crystallization and grain growth in shock-compressed SiO_2," Nat. Commun. **6**, 8191 (2015).
[21]P. Zalden, F. Quirin, M. Schumacher, J. Siegel, S. Wei, A. Koc, M. Nicoul, M. Trigo, P. Andreasson, H. Enquist, M. J. Shu, T. Pardini, M. Chollet, D. Zhu, H. Lemke, I. Ronneberger, J. Larsson, A. M. Lindenberg, H. E. Fischer, S. Hau-Riege, D. A. Reis, R. Mazzarello, M. Wuttig, and K. Sokolowski-Tinten, "Femtosecond x-ray diffraction reveals a liquid–liquid phase transition in phase-change materials," Science **364**, 1062 (2019).
[22]M. Bargheer, N. Zhavoronkov, R. Bruch, H. Legall, H. Stiel, M. Woerner, and T. Elsaesser, "Comparison of focusing optics for femtosecond x-ray diffraction," Appl. Phys. B **80**, 715 (2005).
[23]U. Shymanovich, M. Nicoul, K. Sokolowski-Tinten, A. Tarasevitch, C. Michaelsen, and D. von der Linde, "Characterization and comparison of x-ray focusing optics for ultrafast x-ray diffraction experiments," Appl. Phys. B **92**, 493 (2008).
[24]U. Shymanovich, M. Nicoul, W. Lu, S. Kähle, A. Tarasevitch, K. Sokolowski-Tinten, and D. von der Linde, "Toward ultrafast time-resolved Debye–Scherrer x-ray diffraction using a laser-plasma source," Rev. Sci. Instrum. **80**, 083102 (2009).
[25]F. Zamponi, Z. Ansari, M. Woerner, and T. Elsaesser, "Femtosecond powder diffraction with a laser-driven hard x-ray source," Opt. Express **18**, 947 (2010).
[26]R. Rathore, V. Arora, H. Singhal, T. Mandal, J. A. Chakera, and P. A. Naik, "Experimental and numerical study of ultra-short laser-produced collimated Cu K_α x-ray source," Laser Part. Beams **35**, 442 (2017).
[27]M. Schollmeier, T. Ao, E. S. Field, B. R. Galloway, P. Kalita, M. W. Kimmel, D. V. Morgan, P. K. Rambo, J. Schwarz, J. E. Shores, I. C. Smith, C. S. Speas, J. F. Benage, and J. L. Porter, "Polycapillary x-ray lenses for single-shot, laser-driven powder diffraction," Rev. Sci. Instrum. **89**, 10F102 (2018).
[28]F. Zamponi, P. Rothhardt, J. Stingl, M. Woerner, and T. Elsaesser, "Ultrafast large-amplitude relocation of electronic charge in ionic crystals," Proc. Nat. Acad. Sci. U. S. A. **109**, 5207 (2012).
[29]C. Hauf, A.-A. Hernandez Salvador, M. Holtz, M. Woerner, and T. Elsaesser, "Phonon driven charge dynamics in polycrystalline acetylsalicylic acid mapped by ultrafast x-ray diffraction," Struct. Dyn. **6**, 014503 (2019).
[30]A. Cavalleri, C. W. Siders, F. L. H. Brown, D. M. Leitner, C. Tóth, J. A. Squier, C. P. J. Barty, K. R. Wilson, K. Sokolowski-Tinten, M. Horn von Hoegen, D. von der Linde, and M. Kammler, "Anharmonic lattice dynamics in germanium measured with ultrafast x-ray diffraction," Phys. Rev. Lett. **85**, 586–589 (2000).
[31]M. Bargheer, N. Zhavoronkov, Y. Gritsai, J. C. Woo, D. S. Kim, M. Woerner, and T. Elsaesser, "Coherent atomic motions in a nanostructure studied by femtosecond x-ray diffraction," Science **306**, 1771–1773 (2004).
[32]M. Nicoul, U. Shymanovich, A. Tarasevitch, D. von der Linde, and K. Sokolowski-Tinten, "Picosecond acoustic response of a laser-heated gold-film studied with time-resolved x-ray diffraction," Appl. Phys. Lett. **98**, 191902 (2011).
[33]T. G. White, P. Mabey, D. O. Gericke, N. J. Hartley, H. W. Doyle, D. McGonegle, D. S. Rackstraw, A. Higginbotham, and G. Gregori, "Electron-phonon equilibration in laser-heated gold films," Phys. Rev. B **90**, 014305 (2014).
[34]H. Park, X. Wang, S. Nie, R. Clinite, and J. Cao, "Mechanism of coherent acoustic phonon generation under nonequilibrium conditions," Phys. Rev. B **72**, 100301 (2005).
[35]M. Harb, W. Peng, G. Sciaini, C. T. Hebeisen, R. Ernstorfer, M. A. Eriksson, M. G. Lagally, S. G. Kruglik, and R. J. D. Miller, "Excitation of longitudinal and transverse coherent acoustic phonons in nanometer free-standing films of (001) Si," Phys. Rev. B **79**, 094301 (2009).
[36]A. Feist, N. Rubiano da Silva, W. Liang, C. Ropers, and S. Schäfer, "Nanoscale diffractive probing of strain dynamics in ultrafast transmission electron microscopy," Struct. Dyn. **5**, 014302 (2018).
[37]S. Bastiani, A. Rousse, J. P. Geindre, P. Audebert, C. Quoix, G. Hamoniaux, A. Antonetti, and J. C. Gauthier, "Experimental study of the interaction of subpicosecond laser pulses with solid targets of varying initial scale lengths," Phys. Rev. E **56**, 7179 (1997).
[38]W. Lu, M. Nicoul, U. Shymanovich, A. Tarasevitch, P. Zhou, K. Sokolowski-Tinten, D. von der Linde, M. Mašek, P. Gibbon, and U. Teubner, "Optimized K_α x-ray flashes from femtosecond-laser-irradiated foils," Phys. Rev. E **80**, 026404 (2009).
[39]The used tape target has been developed at the Institute for Quantum Electronics of the Friedrich-Schiller-Universität Jena.[40] The target consists of a 10 μm thick Cu tape mounted on a motorized spooling system, which works similarly to an audiocassette recorder. The pulling speed is approximately 8 mm/s to ensure that fresh surface area is provided for each laser pulse. The tape shifts vertically to its pulling direction by about 0.8 mm when the pulling direction is (automatically)

changed. One set of tape (25 mm wide and 15 m long) can provide more than 12 h of experiment time. In order to minimize the deposition of the ablated material, 8 μm Kapton foil has been rolled together with the Cu tape before mounting it to the spooling system. The Kapton foil runs simultaneously with the tape to pick up the debris which is predominantly ejected at the backside of the tape normal to its surface. Close to the laser-target interaction point, it is mechanically separated from the Cu tape by about 2 mm. The whole target assembly is mounted in a small vacuum chamber at a base pressure of about 0.1 mbar. Measurements of the total Kα yield, the Kα-flux at the sample position (i.e., after the x-ray optic), and the emission spectra have been performed using a thinned, back-illuminated CCD with known quantum efficiency[41] in the photon counting mode, where a single x-ray photon produces a charge in the detecting pixel which is proportional to the photon energy.[42] Further details of the experimental setup and its characterization will be presented in a separate publication.

[40]A. Lübcke, "Time-resolved x-ray diffraction study on superconducting $YBa_2Cu_3O_7$ epitaxially grown on $SrTiO_3$," Ph.D. thesis, Faculty of Physics and Astronomy, Friedrich-Schiller-Universität Jena, 2007.

[41]S. Hubert and V. Prévot, "Quantum efficiency measurements of an x-ray charge-coupled device in the 2–9 keV spectral region by means of a double crystal monochromator coupled to an x-ray tube," Appl. Opt. **53**, 8078–8085 (2014).

[42]F. Zamponi, T. Kämpfer, A. Morak, I. Uschmann, and E. Förster, "Characterization of a deep depletion, back-illuminated charge-coupled device in the x-ray range," Rev. Sci. Instrum. **76**, 116101 (2005).

[43]See www.rigaku.com/en/products/optics/cmf for Manufacturer: OSMIC—Rigaku.

[44]W. Lu, M. Nicoul, U. Shymanovich, A. Tarasevitch, M. Kammler, M. Horn-von Hoegen, D. von der Linde, and K. Sokolowski-Tinten, "Extreme phonon softening in laser-excited bismuth—Towards an inverse Peierls-transition," MRS Proc. **1230**, 1230–MM03–05 (2009).

[45]W. Lu, "Ultrafast time-resolved X-ray diffraction using an optimized laser-plasma based x-ray source," Ph.D. thesis, Faculty of Physcis, University of Duisburg-Essen, 2013.

[46]Manufacturer: Lebow Company. The Ni-mesh had a pitch of 0.36 mm, a (squared) opening of 0.34 mm and, therefore, 0.02 mm bar width.

[47]P. Scherrer, "Bestimmung der Größe und der inneren Struktur von Kolloidteilchen mittels Röntgenstrahlen," Nachr. Ges. Wiss. Goettingen, Math.-Phys. **1918**, 98–100.

[48]The experimental peak width $\Delta\Theta_{exp} \approx 0.7^\circ$ has three different contributions, namely, due to the finite x-ray spot size (converted into angle) on the sample $\Delta\Theta_{spot}$, due to the bandwidth of the radiation reflected by the x-ray mirror $\Delta\Theta_{bw}$, and due to the finite grain size $\Delta\Theta_{gr}$. We assume here that $\Delta\Theta^2_{exp} = \Delta\Theta^2_{spot} + \Delta\Theta^2_{bw} + \Delta\Theta^2_{gr}$. The x-ray spot size on the sample (140 μm FWHM) makes at the large diffraction angles of the (220)- and (311)-reflections, only a small (almost negligible) contribution of $\Delta\Theta_{spot} < 0.1^\circ$. The bandwidth contribution is estimated from the energy difference in the spin-orbit-split Kα1 and Kα2 lines of $\Delta E = 20$ eV (at an average photon energy of EX = 8.03 keV) as $\Delta\Theta_{bw} = 2\Delta E/E_X \cdot \tan(\Theta_B)$ (Θ_B: Bragg-angle). This results in $\Delta\Theta_{bw} \approx 0.2^\circ$ and, therefore, $\Delta\Theta_{gr} \approx 0.66^\circ$. This yields a grain size of about 17 nm. Such a small grain size, much smaller than the film thickness, is in line with the observation of smooth, continuous diffraction rings.

[49]The limited accuracy of the experiment did not allow us to determine the reduction of the Bragg-peak intensities due to the Debye–Waller effect. In fact, using published temperature-dependent Debye–Waller factors for Au,[50,51] the reduction of the peak intensity expected for a temperature rise of 61 K is only 4% for the (311)-reflection, the highest order reflection we did measure.

[50]V. Syneček, H. Chessin, and M. Simerska, "The temperature dependence of lattice vibrations in gold from X-ray diffraction measurements," Acta Crystallogr., Sect. A **26**, 108 (1970).

[51]H. X. Gao and L.-M. Peng, "Parameterization of the temperature dependence of the Debye–Waller factors," Acta Crystallogr., Sect. A **55**, 926 (1999).

[52]O. B. Wright, "Ultrafast nonequilibrium stress generation in gold and silver," Phys. Rev. B **49**, 9985 (1994).

[53]C. Thomsen, H. T. Grahn, H. J. Maris, and J. Tauc, "Surface generation and detection of phonons by picosecond light pulses," Phys. Rev. B **34**, 4129 (1986).

[54]*CRC Handbook of Chemistry and Physics*, edited by D. R. Lide (CRC Press, 2005).

[55]S. Anisimov, B. Kapeliovich, and T. Perel'man, "Electron emission from metal surfaces exposed to ultrashort laser pulses," Sov. Phys. JETP **39**, 375 (1974).

[56]K. Sokolowski-Tinten, X. Shen, Q. Zheng, T. Chase, R. Coffee, M. Jerman, R. K. Li, M. Ligges, I. Makasyuk, M. Mo, A. H. Reid, B. Rethfeld, T. Vecchione, S. P. Weathersby, H. A. Dürr, and X. J. Wang, "Electron-lattice energy relaxation in laser-excited thin-film Au-insulator heterostructures studied by ultrafast MeV electron diffraction," Struct. Dyn. **4**, 054501 (2017).

[57]J. Hohlfeld, J. Müller, S.-S. Wellershoff, and E. Matthias, "Time-resolved thermoreflectivity of thin gold films and its dependence on film thickness," Appl. Phys. B **64**, 387 (1997).

[58]J. Hohlfeld, S.-S. Wellershoff, J. Güdde, U. Conrad, V. Jähnke, and E. Matthias, "Electron and lattice dynamics following optical excitation of metals," Chem. Phys. **251**, 237 (2000).

[59]T. Barron, J. Collins, and G. White, "Thermal expansion of solids at low temperatures," Adv. Phys. **29**, 609 (1980).

[60]O. L. Anderson, D. G. Isaak, and S. Yamamoto, "Anharmonicity and the equation of state for gold," J. Appl. Phys. **65**, 1534 (1989).

DOI: 10.1063/1.5142220
URN: urn:nbn:de:hbz:464-20200709-114927-1